A composite view of ozone evolution in the 1995-96 northern winter polar vortex developed from airborne lidar and satellite observations

A. R. Douglass, M. R. Schoeberl and S. R. Kawa
NASA Goddard Space Flight Center

E. V. Browell
NASA Langley Research Center

Short title:

Abstract. The processes which contribute to the ozone evolution in the high latitude northern lower stratosphere are evaluated using a three dimensional model simulation and ozone observations. The model uses winds and temperatures from the Goddard Earth Observing System Data Assimilation System. The simulation results are compared with ozone observations from three platforms: the differential absorption lidar (DIAL) which was flown on the NASA DC-8 as part of the Vortex Ozone Transport Experiment; the Microwave Limb Sounder (MLS); the Polar Ozone and Aerosol Measurement (POAM II) solar occultation instrument. Time series for the different data sets are consistent with each other, and diverge from model time series during December and January. The model ozone in December and January is shown to be much less sensitive to the model photochemistry than to the model vertical transport, which depends on the model vertical motion as well as the model vertical gradient. We evaluate the dependence of model ozone evolution on the model ozone gradient by comparing simulations with different initial conditions for ozone. The modeled ozone throughout December and January most closely resembles observed ozone when the vertical profiles between 12 and 20 km within the polar vortex closely match December DIAL observations. We make a quantitative estimate of the uncertainty in the vertical advection using diabatic trajectory calculations. The net transport uncertainty is significant, and should be accounted for when comparing observations with model ozone. The observed and modeled ozone time series during December and January are consistent when these transport uncertainties are taken into account.

1. Introduction

The annual springtime loss of ozone in the high southern latitude lower stratosphere known as the ozone hole was discovered by *Farman et al.* [1985]. There is now general consensus that catalytic loss cycles involving chlorine and bromine radicals are responsible for this ozone loss [e.g., *Solomon et al.*, 1990; *Anderson et al.*, 1991; *Albritton et al.*, 1995]. The losses follow release of chlorine radicals from reservoir gases HCl and $ClONO_2$ through heterogeneous reactions on the surfaces of cloud particles which form at low temperature in the polar lower stratosphere. Both in situ measurements of ClO from aircraft [e.g., *Brune et al.*, 1990] and observations of ClO from the Upper Atmosphere Research Satellite (UARS) Microwave Limb Sounder (MLS) [*Waters et al.*, 1995] show that the mixing ratio of ClO in the northern high latitude winter lower stratosphere is comparable to the maximum ClO mixing ratio observed in the southern hemisphere for at least part of most northern winters. However, as shown by *Newman et al.* [1997], although the March average of the total ozone observed between 63°N and 90°N by Total Ozone Mapping Spectrometers (TOMS) has decreased during the 1990's, the annual spring loss of northern hemisphere ozone has not equaled the annual southern loss. The northern hemisphere vortex is not as cold or long lasting as the southern vortex. The lowest March total ozone for the 20 years of observations which were made between the 1970's through 1997 was observed in 1997, a year when the northern polar vortex was unusually cold and persistent [*Coy et al.*, 1997]. Models are challenged to predict the future northern hemisphere ozone loss, and to identify the

conditions of climate and trace gas abundance for which extreme ozone loss is likely to occur.

The principle difficulty in quantifying ozone losses from observations or in testing simulations is the need to account for both transport processes and photochemical processes. In the winter lower stratospheric polar vortex, the continuity equation for ozone can be approximated

$$\frac{\partial \overline{\gamma}_{O3}}{\partial t} = -\overline{L} - \overline{w}^{*}\frac{\partial \overline{\gamma}_{O3}}{\partial z} \qquad (1)$$

where γ_{O3} is the ozone mixing ratio, L is photochemical loss, w^{*} is the residual vertical velocity and the overbar indicates the zonal average. Photochemical ozone production is negligible in the winter polar lower stratosphere, and is not included in Equation 1. Horizontal transport and mixing are also neglected. There is general downward (negative) vertical motion for the high latitude winter [*Rosenfield et al.*, 1994]; since ozone increases with altitude in the lower stratosphere, descent tends to increase ozone. Significant photochemical loss through catalytic cycles involving chlorine radicals is possible in sunlit air when heterogeneous reactions have altered the balance of chlorine constituents away from reservoirs HCl and $ClONO_2$.

Under usual conditions in the northern hemisphere winter, diabatic descent increases ozone near the poles. The highest column ozone amounts usually observed anywhere are found near the north pole during spring. However, recently the polar ozone maximum has weakened [*Newman et al.*, 1997]. Part of this decrease is due to

photochemical loss processes involving chlorine species, but if the diabatic descent is weak then the ozone build-up is also reduced. The two processes tend to work together to decrease ozone, and years with weak diabatic descent are also years when the polar vortex is cold. *Lefevre et al.* [1998] show good agreement of TOMS observations with total ozone calculated from a 3D CTM with meteorological input from the European Centre for Medium Range Weather Forecasts (ECMWF), and find that photochemical and transport processes make comparable contributions to the low ozone in spring 1997.

There have been efforts to estimate the photochemical loss from observations. *Schoeberl et al.* [1990] inferred the ozone loss from observations of ozone and nitrous oxide, using the nitrous oxide to account for transport. *Müller et al.* [1997] used observations of HF and O_3 from the UARS Halogen Occultation Experiment (HALOE) to evaluate the ozone loss over the course of the winter, under the assumption that the early winter relationship between these two constituents would be unchanged in the absence of photochemical loss. *Manney et al.* [1994; 1996] used trajectory calculations to account for descent due to diabatic cooling in deriving the chemical ozone loss from MLS ozone observations. *Rex et al.* [1998; 1999] calculated ozone loss from ozone sonde measurements using trajectory calculations to match observations in the same airmass a few days apart. This analysis shows a larger photochemical ozone loss during January 1992 than can be accounted using box model calculations [*Becker et al.*, 1998]. Using a 3D CTM driven by ECMWF analyses to account for transport by treating an ozone like field as a conserved tracer, *Goutail et al.* [1999] derive an estimate for ozone loss during the 1994-95 northern winter from ground based and balloon measurements. *Deniel et al.*

[1998] use the same model results to derive an estimate of loss from ozone observations made by the Polar Ozone and Aerosol Measurement (POAM II) on board the French Satellite Pour l'Observations de la Terre. Both of these results suggest more rapid ozone chemical loss during December and January than is produced by the photochemical model. These results and those of *Becker et al.* [1998] and *Rex et al.* [1998; 1999] suggest that there may be an unaccounted loss process for ozone which is active in low sunlight. However, use of a conservative ozone-like tracer from a CTM to estimate ozone loss from observations makes the assumption that the CTM accurately simulates the actual atmospheric transport. Any systematic difference between modeled ozone and observations produced by a difference between actual and modeled transport could be attributed to a deficiency in model photochemistry. *Goutail et al.* [1999] address the validity of the model descent by comparing a small number of observed N_2O profiles with model profiles, and find that modeled differential descent is realistic. However, this comparison at best evaluates net descent over the winter, and does not verify the temporal dependence of the descent.

There is less difficulty in quantifying ozone loss when the transport contribution to the ozone tendency is small. For example, *Wu and Dessler* [2000] show good agreement for the southern hemisphere lower stratosphere between the ozone tendency calculated from MLS ozone and the ozone tendency calculated using MLS ClO, when radiative calculations show that descent is unimportant to the ozone tendency.

The analysis presented here is focussed on the ozone change from early to mid-winter (early December to the end of January and the beginning of February). We utilize

observations from three platforms, the UV differential absorption lidar (DIAL), POAM II and UARS MLS. The observations from each platform are compared with an ozone simulation from the GSFC three dimensional chemistry and transport model, which uses winds and temperatures from the Goddard Earth Observing System Data Assimilation System (GEOS DAS). Like the results of *Deniel et al.* [1998], these comparisons show a departure of modeled ozone from observations that grows from early to midwinter.

Each data set provides unique information to the analysis. Several flights of the DC-8 during early and midwinter either penetrate deeply or cross the polar vortex. DIAL ozone profiles show that ozone is uniform along the flight track. These high vertical resolution profiles are used to calculate the ozone vertical gradient. POAM II provides about 11 profiles near 65°N most days throughout the winter, and the near continuous sampling is used to evaluate any seasonal (sunlight) dependence of the departure. MLS provides profiles of O_3 and ClO throughout the northern hemisphere most days between November 25 and December 25, 1995 and between January 29 and February 29, 1996. The MLS O_3 observations are used to show that the departure of observed and modeled ozone is consistent throughout the vortex. The MLS ClO observations are used to verify the modeled evolution of reactive chlorine.

There are two principle goals to this paper. The first goal is to use the complementary aspects of the three data sets to characterize differences between the modeled ozone evolution and that inferred from the observations. The second goal is to evaluate the sensitivity of model ozone to the modeled photochemical and advective processes. The sensitivity of model results to total inorganic chlorine is used to estimate

the sensitivity to photochemical processes. The sensitivity to vertical advection is determined by comparing results for calculations with different profiles for early winter ozone, and by comparing the model net vertical transport for 15 day periods with that expected from diabatic trajectory calculations. Over a two month period the uncertainty in vertical transport is comparable to the difference in the modeled and observed ozone evolution. Our calculations do not support the existence of an unexplained midwinter ozone loss mechanism.

The data sets and data analysis procedures used in this study are described in the following section. The CTM and a description of the simulations are given in section 3. The trajectory model and its application to this study are also described in section 3. The comparison of a base case ozone simulation with observations is given in section 4. Section 5 contains a discussion of the results and evaluation of the sensitivity of the ozone evolution to the contributing photochemical and transport terms. A summary and conclusions are given in section 6.

2. DATA

2.1 DIAL

The DIAL lidar was flown on the DC-8 during the northern 1995-96 winter as part of the Vortex Ozone Transport Experiment (VOTE) and the Tropical Ozone Transport Experiment (TOTE). The first segment of these missions took place in December

1995, with the second segment in late January and early February 1996. The DIAL system is used to measure aerosol, cloud, and ozone profiles above the DC-8 aircraft [*Browell et al.*, 1998]. The measurement is made from the aircraft altitude (~12 km) to about 25 km with an accuracy of better than 10%. Measurements are reported as 5 minute averages of the data (about every 70 km) and the vertical resolution is 750 m. Correlative measurements with ground based systems showed good agreement [*Grant et al.*, 1998].

The VOTE and TOTE missions were planned to examine small scale features in ozone and methane to determine the importance of such features to exchange of gases between the midlatitudes and the polar vortex (VOTE) or the tropics (TOTE). Flights of the DC-8 at middle and high northern latitudes during the first half of December (early winter) and January 24, 1996 - February 8, 1996 (midwinter) are listed in Table 1.

DIAL data are reported on a pressure altitude and time grid. The data are interpolated onto isentropic surfaces based upon UKMO analyses. At the highest altitudes, the DIAL data becomes more uncertain because the backscatter signal weakens due to decreasing molecular density, and as the signal is absorbed by the intervening ozone layer. The altitude limit on DIAL observations thus decreases with increasing latitude as the ozone layer descends.

2.2 Polar Ozone and Aerosol Measurements

The Polar Ozone and Aerosol Measurement (POAM II) solar occultation instrument, on board the French Satellite Pour l'Observations de la Terre (SPOT 3)

measured ozone profiles at about 12 longitudes at each of two latitudes daily between October 15, 1993 and November 14, 1996. The instrument is described in detail by *Glaccum et al.* [1996]. Ozone number density profiles are retrieved with 1 km vertical resolution between 10 and 60 km altitude. For the version 5 retrieval used here, both random and systematic errors are estimated to be 5% or less between 10 and 50 km [*Lumpe et al.*, 1997]. For this work, temperature and pressure from the National Center for Environmental Prediction (NCEP) are used to convert measured concentrations to volume mixing ratios, and to interpolate the mixing ratio profiles to potential temperature surfaces. Between November 16, 1995 through February 29, 1996 the measurement latitude varies between 62°N and 68°N.

2.3 Microwave Limb Sounder

The UARS MLS observes from 34° latitude in one hemisphere to 80° latitude in the opposite hemisphere for periods of about one month [*Reber et al.*, 1993]. The MLS instrument is described by *Barath et al.* [1993]. The ozone data used here are from the 205 GHz radiometer; ozone mixing ratio profiles at UARS pressures are retrieved using the version 4 algorithm. MLS reports observations on alternate UARS standard pressure levels, including 100, 46, and 22 hPa. Validation for the version 3 algorithm is discussed by *Froidevaux et al.* [1996]. The version 4 algorithm is somewhat improved at 46 hPa, where the estimated accuracy is 20% for version 4 compared with 30% for the version 3. The single profile precision is estimated to be 11% (0.2 ppmv) for both retrievals. At 100 hPa the estimated accuracy is about 50% and the single profile

precision is also greater than 50% for both version 3 and version 4. Only the 500 K potential temperature surface is utilized for comparisons of model O_3 with MLS data because of the lower accuracy at 100 hPa compared with that reported for the other instruments.

Waters et al. [1996] provide validation for ClO data obtained using the version 3 algorithm. There are two errors in the version 3 ClO retrieval which are removed in version 4. These are an 8% scaling error and a high bias whenever climatological HNO_3 used in the retrieval greatly exceeds the actual atmospheric (gas phase) HNO_3; this is the case in the high-latitude winter lower polar stratosphere when HNO_3 is often in a condensed phase [*Santee et al.*, 1996]. Version 4 data are used here. At 46 hPa the single profile 1-sigma precision for ClO is 0.5 ppbv; the estimated accuracy is 10%.

Temperature profiles coincident with the MLS observations are from the NCEP analysis, as the MLS temperature measurement is not valid at higher pressure than 21.5 hPa. The NCEP temperature profiles are used to interpolate the MLS ozone and chlorine monoxide profiles to the 500K potential temperature surface. MLS sees high northern latitudes for 24 days between November 25 and December 25, for January 29-31 and 12 days between February 13 and and February 29, 1996.

2.4 Analysis Methods

The spatial and temporal sampling patterns for the DC-8 DIAL lidar, POAM, and the UARS MLS differ, as illustrated in Plate 1a, which superposes the locations of observations from each of the instruments on January 30, 1996 on the model N_2O

field at 500 K. The model N_2O shows the sharp contrast between middle latitudes and the polar vortex, and a strong correlation with 500K potential vorticity (Plate 1b). The DC-8 flight track for January 30 (the solid black line between 220° and 280° longitude near 67°N) crosses the highest N_2O gradient. POAM (white filled circles) observes both vortex and non-vortex air near this same latitude. MLS (small purple 'x') has the highest spatial sampling; the separation of observations in longitude varies with latitude. Model comparisons with data are accomplished by sampling the model in the same way as the observing platform. To make the most effective comparisons among the platforms, we utilize the strong correlation of long-lived constituents with potential vorticity [*Schoeberl and Lait*, 1992]. A single day's data and model output are interpolated to specified potential temperature surfaces and averaged using potential vorticity to account for horizontal structure. Equivalent latitude θ_E is calculated as described by *Nash et al.* [1996] by associating the area enclosed by a potential vorticity contour with the area poleward of θ_E. Binning and averaging points based on a given range of potential vorticity permits formation of time series by averaging model or observations at locations with similar transport and photochemical histories, while accounting for changes in vortex shape and intensity.

3. Models

3.1 GSFC Chemistry and Transport Model

The chemistry and transport model (CTM) used here is an improved version of that used to analyze observations from UARS MLS, Cryogenic Limb Array Etalon Spectrometer (CLAES), and HALOE [*Kawa et al.*, 1995; *Douglass et al.*, 1997] and NIMBUS 7 TOMS [*Douglass et al.*, 1996]. Model winds and temperatures are taken from a version of GEOS DAS which is described in the Algorithm Theoretical Basis Document of the Data Assimilation Office [*DAO,* 1997]. Relevant aspects of changes in the assimilation system used here over that used in previous applications of this model are described by *Douglass and Kawa* [1999], which also contains a more complete description of the CTM. Briefly, the transport contribution to the constituent continuity equation is solved using a scheme developed by *Lin and Rood* [1996]. This scheme maintains sharp gradients and appropriate correlations for long-lived constituents, and does not produce unrealistic maxima or minima. The photochemical scheme includes all gas phase reactions thought to be important in the stratosphere; rate constants are taken from *DeMore et al.* [1994]. Six heterogeneous reactions are included: N_2O_5, $ClONO_2$, and $BrONO_2$ with H_2O, and N_2O_5, $ClONO_2$, and HOCl with HCl. The sulfate surface area distribution for a volcanically clean atmosphere is taken from the *Scientific Assessment of Ozone Depletion: 1991* [*Albritton and Watson*, 1992]. The heterogeneous scheme is the same as used by *Kawa et al.* [1997], which shows good agreement with chlorine activation data and is essentially the same as given by *DeMore et al.* [1997].

Photolysis rates are calculated using temperature dependent cross sections [*DeMore et al.*, 1994] and reduced fluxes interpolated from a table-lookup based on the detailed radiative transfer calculations [*Anderson and Lloyd*, 1990]. These photolysis rates compare favorably with the photolysis benchmark which was developed as part of the Atmospheric Effects of Aviation Project [*Stolarski et al.*, 1995]. This photochemical scheme is used in the CTM and also to calculate chemical evolution along trajectories initialized with 3D model fields. Updates to photochemical input data subsequent to *DeMore et al.* [1997] are not important to this study.

Three simulations for the November 15, 1995 - March 1, 1996 are compared with observations and contrasted with each other in the following sections. These simulations are identical in their meteorological fields and photochemical scheme, but differ in their initialization of ozone and inorganic chlorine in the high latitude lower stratosphere. Case I follows the initialization procedure described by *Douglass et al.* [1997]. A two dimensional average field of N_2O is constructed by binning October and November 1992 observations from CLAES using potential vorticity to define the horizontal coordinate and potential temperature for the vertical coordinate. An average ozone field is defined in the same way, using MLS observations from November 10-11 and November 25-26 1995. These fields are mapped onto a three dimensional grid, using potential temperature as the vertical coordinate and potential vorticity for November 15, 1995 to define the horizontal structure. Ozone in the lower stratosphere and the remaining long lived constituents and families are taken from the GSFC two dimensional model [*Jackman et al.*, 1996] and mapped onto the 3D grid using N_2O as the vertical

coordinate.

It is instructive to compare the model fields after a few weeks integration with observations, and to compare the observations with each other. Data are binned and averaged as described in section 2.4. The average profiles from MLS and POAM for all observations between 72°N and 76°N equivalent latitude from December 1-10 are shown in Plate 2a, with the average profile for the DC-8 flight on December 9. At and below 20 km, there are differences among the observations. The differences among the observed profiles are more informative when the vertical gradients are compared. These are given in Plate 2c. The vertical gradient of the average POAM profile is close to that derived from DIAL up to about 19 km. Above 19 km, the DIAL vertical gradient is smaller than that derived from POAM. The vertical gradient of MLS is smaller than POAM at all altitudes shown, probably because the vertical resolution of MLS is much larger than that of POAM.

The average of the model fields sampled for the same period as by satellite or aircraft are also shown in Plate 2a. The model profiles (dashed lines) are similar to each other regardless of sampling, which is expected as the model ozone field is fairly uniform within the polar vortex. Above 20 km Case I model ozone is up to 1 ppmv too high. The model O_3 within the polar vortex in early December is very close to the zonal mean for the initial condition, suggesting that the initialization which is made when the vortex is forming does not capture the contrast in ozone profiles between vortex and non vortex air.

The Case II initialization for ozone was purposely derived to be closer to the DIAL

December vortex profiles. MLS profiles for a longer time window (November 25 - 30, 1995) were binned to define the relationship of ozone and potential vorticity, giving better separation vortex and non vortex profiles at high latitude. The profiles with higher potential vorticity on November 15 are altered from the Case I initialization. The comparisons of model output with observations as in Plate 2a are given for the Case II initialization in Plate 2b. Model output is in better agreement with respect to the overall shape of the observed profiles.

These vertical gradients for both initializations are compared with observed vertical gradients in Plates 2c and 2d. Between 17 and 24 km the model vertical gradient for Case I initialization exceeds that calculated from all of the data sets. Near 20 km the discrepancy is as much as 0.4 ppmv per kilometer. Even for weak downward motion, this gradient difference can significantly alter the polar ozone distribution over the winter. For the Case II initialization the model vertical gradient (Plate 2d) approximates the DIAL vertical gradient more closely than for Case I, but the model vertical gradient still exceeds the DIAL vertical gradient near 500K. The Case II initialization more closely approximates MLS and POAM vertical gradients above 500K; note that the vertical gradients from POAM and MLS are larger than DIAL at 500K. Because the assimilation winds do not exactly represent atmospheric motion, model fields are unlikely to exactly match observations on December 9 from any initialization on November 15. For the same reason, it is practical to consider a difference in the shape of modeled and observed profiles as a source of uncertainty in the modeled ozone tendency.

The model ozone tendency for early to midwinter in the lower stratosphere may

also be sensitive to photochemical loss, in particular to catalytic cycles involving chlorine radicals which have been released from reservoir species HCl and $ClONO_2$ through heterogeneous reactions. The average of sunlit ClO observations from MLS, with potential vorticity greater than that at equivalent latitude 70°N, is compared with the model average for ClO inferred from ClO_x=ClO + Cl_2O_2 + OClO in Figure 1. It is necessary to infer ClO because the model output are saved only every six hours. The model captures the temporal evolution of the observed ClO, and is generally within the standard deviation of the MLS mean. This comparison provides confidence that the chemical contribution to the ozone evolution from the modeled chlorine species will exhibit the appropriate temporal dependence. To test the sensitivity of the results to the total chlorine, a third initial condition was developed (Case III) which is identical to Case II except there is a 10% increase in total chlorine (and thus the total ClO_x and daytime ClO) in the high latitude lower stratosphere. This enhancement can be thought of as a proxy for changes in photolysis rates or reaction rates that would speed up chlorine catalyzed ozone loss cycles. The impact of these different initializations on the comparisons of the model simulations with observations are discussed in Section 5.

3.2 Evaluation of CTM Vertical Transport

Weaver et al. [1993] show that the overall vertical transport in a CTM in which the vertical velocity is calculated from the horizontal divergence for each grid box is consistent with the residual vertical velocity calculated from the definition given by *Andrews and McIntyre* [1976]

$$\overline{w}^* = \overline{w} + \frac{1}{r cos\phi} \frac{\partial \cos\phi \, \overline{v'\Theta'}}{\partial \phi} \left(\frac{\partial \overline{\Theta}}{\partial z} \right)^{(-1)} \tag{2}$$

Here Θ is the potential temperature, v is the meridional velocity, ϕ is the latitude, the overbar indicates the zonal mean and primes indicate the deviation from the zonal mean. Because the residual thermodynamic equation takes the approximate form

$$\frac{\partial \overline{\Theta}}{\partial t} + \overline{w}^* \frac{\partial \overline{\Theta}}{\partial z} = \overline{Q} \tag{3}$$

where $\overline{Q}$ is the diabatic heating rate [*Dunkerton*, 1978], the residual vertical velocity can also be written

$$\overline{w}^* = \frac{\overline{Q} - \partial \overline{\Theta} / \partial t}{\partial \overline{\Theta} / \partial z}. \tag{4}$$

In the assimilation process observations are combined with a general circulation model (GCM) every six hours. The residual circulation is produced by the analysis system, the observations, and the underlying GCM, and there is no constraint which requires equivalence of the residual vertical velocity computed from (2) with that computed using (4). In fact, noise in the assimilation fields will strongly impact $\overline{w}^*$ when (2) is used compared to $\overline{w}^*$ computed from (4). Because the CTM is not constrained to follow the residual circulation as derived from (4), there is a possibility of a systematic difference in the vertical transport. Such errors have prompted *Chipperfield* [1999] to develop an isentropic CTM in which the only vertical motion is calculated from the diabatic heating. This approach has the advantage that the vertical motion is consistent with the heating rates, but the disadvantage that there may be inconsistency between

the horizontal divergence and the vertical motion, requiring an adjustment to maintain mass conservation.

There are various approaches to verify the vertical transport in a CTM, such as comparisons of model N_2O profiles with observations inside and outside the vortex [*Goutail et al.*, 1999]. However, the temporal evolution of vertical transport cannot be evaluated from a few profiles. For the three N_2O profiles used by *Goutail et al.* [1999], the measurement uncertainty in the lower stratosphere is significant compared to the difference between the vortex and extra vortex profiles. Therefore, such comparisons do not eliminate the possibility of errors in the lower stratospheric downward motion. There are no tracer profiles which would fully validate the downward motion during early to midwinter 1995-96.

One approach to evaluating the modeled vertical motion is to compute the vertical motion from the thermodynamic equation utilizing diabatic trajectory calculations. The vertical motion computed from the heating rate is a function of temperature and small fluctuations in temperature do not create large fluctuations in the heating rates. The Lagrangian (trajectory) calculation also eliminates the possibility of numerical mixing associated with fixed grid point calculations.

Diabatic back trajectories were calculated for the 400K, 450K and 500K surfaces for a grid of points (5° latitude by 4° longitude). Meteorological fields were taken from GEOS DAS and from United Kingdom Meteorological Office (UKMO). Heating rates are provided as part of the GEOS DAS analysis. Heating rates for UKMO meteorological fields are calculated off line [*Rosenfield et al.*, 1994]. The vertical

displacement of parcels from the trajectories is compared with the net vertical advection produced by the CTM utilizing model fields of N_2O. Diabatic estimates for fields of N_2O are constructed by mapping the 3D model field for the final day of the back trajectory calculation to the initial regular grid. A comparison of a constructed field with the model field on a particular day provides an estimate of the consistency of the CTM vertical transport with the heating rates over the time period of the trajectory calculation. This comparison is used to identify and quantify systematic errors in the model transport that affect the model ozone tendency.

A second application of the trajectory model is to calculate chemical evolution for O_3 and other reactive gases along these trajectories. The calculations use the same integration scheme as the CTM and are initialized by interpolating the CTM fields to the location (longitude, latitude, potential temperature) of each parcel at the terminus of the back trajectory calculation. This allows a rapid test of sensitivity to various photochemical processes.

4. Model Data Comparisons

For comparisons of the model with observations, the observations and model output are averaged for 4° bins of equivalent latitude as described in section 2.4. The differences between model O_3 and observations poleward of 66°N equivalent latitude are shown for the 400K, 450K, and 500K potential temperature surfaces for DIAL (Plate 3 a-c), POAM (Plate 3 d-f), and MLS (Plate 3g).

The DIAL observations are limited to two observing periods (Table 1). The

average differences between the model and observation shown in Plate 3a-c are larger in January/February than December at all three potential temperature surfaces. There are observations in most equivalent latitude bins during both periods. The differences during each time period do not exhibit organized dependence on equivalent latitude.

The POAM observations are nearly continuous throughout the winter. All but the highest equivalent latitude bins are frequently represented in the time series in Plate 3 d-f. The time series for the differences model - POAM are not inconsistent with the model - DIAL time series, but present a somewhat different picture. At 400K, the difference between model and observation peaks in middle January and decreases thereafter. At 450K and 500K the difference increases nearly linearly between December 15 and late January. These differences are similar to differences reported by *Deniel et al.* [1997] comparing POAM ozone with a CTM simulation using ECMWF meteorological fields.

The MLS observations are limited to three periods, one in December, the second in late January and the third in the second half of February. At 500 K, all equivalent latitude bins are represented daily. Like comparisons of the model with DIAL and POAM, the difference between the model and MLS is much larger in midwinter than in early winter. The difference between the model and MLS grows throughout the time period.

The comparisons of the simulation with observations from DIAL, POAM and MLS given in Plate 3 are consistent for all three potential temperature surfaces, and are summarized for the 500K surface in Figure 2. The mean differences between model and

observations at 500K are given for all observations in December (Figure 2a) and for midwinter (January 24 - February 19, Figure 2b). In December, the difference between model and MLS observations ($\sim$ 0.4 ppmv) is nearly independent of equivalent latitude and is consistent with DIAL and POAM comparisons poleward of 66°N. At middle latitudes, the large difference between model and DIAL reflects increased synoptic variability and the coarse model horizontal resolution compared with DIAL data. The comparison of the model with global fields from MLS for December 1-25 is a better estimate of the overall model fidelity. The difference in the means (model - data) for the three data sets are due to biases among the instruments. Poleward of about 60°N equivalent latitude the standard deviation for MLS and DIAL is smaller than at lower latitudes, consistent with less synoptic variability within the polar vortex. At midwinter (Figure 2b), the difference between modeled and observed O_3 at middle latitudes is similar to that in December, but there is a pronounced bias poleward of 62°N equivalent latitude. There is no dependence of the bias on equivalent latitude once past a transition that is approximately the vortex edge.

5. Sensitivity and Possible errors

As noted in section 3.1, the model vertical ozone gradient in the high latitude lower stratosphere in December compares poorly with the vertical gradient determined from DIAL observations for the Case I initialization. The sensitivity of the model ozone at later times to this vertical gradient is evaluated by making the same comparisons with observations for the simulation using the Case II initialization. Reducing the model

vertical gradient early in the integration reduces but does not eliminate the discrepancy between model and observations. The O_3 from the Case II simulation is compared with both MLS and POAM observations at 500K in Figure 3a, which can be compared directly with Plate 3f-g. These comparisons are not differentiated based on equivalent latitude because the discrepancy between model and observation was shown to be uniform across the vortex in the previous section. The agreement between model and observations is improved for the Case II initialization, as expected because of the better agreement of the model profile with DIAL profiles. Comparison of the two model runs shows that there is sensitivity to the initialization for the entire time period (Figure 3b). This is not surprising, since model N_2O within the vortex decreases throughout the period at 500K, indicating descent. Discrepancies at 450K are also reduced by the reduction in vertical gradients as shown in Plate 2.

The difference between the model and POAM at 500K increases steadily between December 15 and January 30, and levels off somewhat during February as the solar insolation increases (Plate 3 and Figure 3). Maximum inorganic chlorine in the model is about 3 ppbv at 500K and is nearly equal to model ClO_x from middle December through late January (Figure 1). The lines in Figure 1 which represent model ClO_x show that model ClOx is nearly independent of equivalent latitude. In February observation and model show that ClO mixing ratios are substantially smaller than during January. The overall model behavior of ClO_x and O_3 is consistent with little ozone loss during early to mid winter due to lack of sun, and competition during February between catalytic destruction of ozone and reformation of the $ClONO_2$ following release of NO_2 from

HNO_3. The same chemical integration scheme was used to calculate the O_3 change along trajectories, initializing the trajectory calculation from the 3D model fields. These calculations for parcels within the polar vortex show that the solar zenith angle is less than 90 fewer than 2 days for each 15 day period between December 1 and January 15. The time for which parcels are sunlit increases steadily thereafter to more than 4 days per 15 days by the end of February. The temporal dependence of the model sensitivity to the total chlorine (Case III - Case II in Figure 3b) reflects the temporal dependence of insolation of high latitude air. For example, the calculated change in O_3 for early to midwinter is not sensitive changes in photochemical input or changes in constituents such as total bromine. Using box model sensitivity to analyze ozone sonde data *Becker et al.* [1998] come to the same conclusion.

In the Case III initialization the total chlorine is increased by 10% throughout the lower stratosphere. As noted above, nearly all of the inorganic chlorine is released from the HCl and $ClONO_2$ reservoirs by late December. As shown in Figure 3b, there is little impact of the Case III initialization on the comparisons of model O_3 with MLS and POAM at 500K. There is almost no sensitivity of model ozone to the total model chlorine until February, and the sensitivity is small compared with the difference between model and observations (Figure 3b). At the end of January the difference between the model ozone and POAM is $\sim$ 0.7 ppmv, and the model O_3 change due to a 10% increase in Cl_Y is less than 0.05 ppmv. The model is more sensitive to Cl_Y in February. By February 15, the difference between the model and POAM or MLS is $\sim$ 0.75 ppmv, and the model O_3 change is $\sim$ 0.1 ppmv due to the 10% increase in Cl_Y.

The sensitivity of the bias between observations and model to the model profile shape prompts the analysis of the model mean vertical transport utilizing diabatic trajectory calculations. The N_2O fields constructed from UKMO and GEOS DAS back trajectories as described in section 3.2 are compared with the CTM N_2O field at 500K in Plate 4a-c for December 31, 1995 and in Plate 4d-f for January 30, 1996. The overall structure of the full model calculation is similar to the field produced with the trajectories, although fields produced by the model Eulerian transport are smoother than the trajectory fields. On December 31, 1995 the CTM N_2O within the polar vortex is lower than the fields constructed from the back trajectories using either GEOS DAS or UKMO input. The differences between the CTM field and the trajectory fields are larger for GEOS DAS input. This is the case for all comparisons until January 30, 1996, when the model and the trajectory calculations give nearly identical results for N_2O within the vortex. Later in February the model tends to underestimate the descent relative to the diabatic calculations. Smaller differences with the same geographic and temporal character are found at 450K. At 400K the trajectory fields are nearly identical to the model fields. This is consistent with the smaller diabatic heating rates and smaller role for vertical transport.

The differences between the model and the trajectory fields in each case estimate the difference in model descent over the 15 days of the back trajectory calculations. Note that non-geophysical horizontal mixing across the vortex edge, absent in the trajectory calculation but possible in the CTM, would increase the N_2O inside the vortex, thus the observation that the model N_2O is lower than the trajectory estimate is not explained

by excess horizontal mixing in the CTM. Noting that the model maintains a transition between the vortex and middle latitudes (Plate 1), we assume that horizontal mixing across the vortex is minimal in the CTM and interpret the difference in N_2O as an uncertainty in the vertical transport. We emphasize that this calculation is made to quantify descent only during midwinter in the lowest part of the stratosphere, after the vortex has already been established.

For a time period t_0 to t_1, the uncertainties in O_3 and N_2O due to vertical advection are given by

$$\Delta N_2O = \Delta\overline{w}^* \frac{\partial N_2O}{\partial z}(t_1 - t_0) \tag{5}$$

$$\Delta O_3 = \Delta\overline{w}^* \frac{\partial O_3}{\partial z}(t_1 - t_0) \tag{6}$$

Assuming that N_2O is conserved, and that the advective and photochemical contributions to the ozone continuity equation can be evaluated separately, the uncertainty in model O_3 due to vertical transport can be quantified by relating the difference in N_2O to the model vertical gradient in O_3 with respect to N_2O:

$$\Delta O_3 \simeq \Delta N_2O \times \frac{\partial O_3}{\partial N_2O} \tag{7}$$

The uncertainties in the vertical transport for the separate 15 day periods are shown in Figure 4a for GEOS DAS winds and heating rates and in Figure 4b for UKMO meteorological fields. The model gradients are calculated from the simulation using

Case II initialization; larger uncertainties would be calculated for the larger O_3 vertical gradient in Case I. The uncertainties are generally negative, and do not show strong dependence on equivalent latitude, with the exception of 66°N for UKMO. The sum of the uncertainties up to a given time interval is an estimate of the error in the ozone up to that time that can be ascribed to vertical transport. These are shown for GEOS DAS in Figure 4c and for UKMO in Figure 4d. The error estimates from UKMO trajectories are smaller than those estimated using GEOS DAS trajectories, but are comparable to the difference in modeled and observed ozone evolution in both magnitude and temporal character in both cases (compare with Figure 3). The difference between UKMO and GEOS DAS reflects the difference in the diabatic heating rates.

The estimated ozone errors are somewhat smaller at 450K; the maximum is about 0.4 ppmv for GEOS DAS and 0.2 ppmv for UKMO. The error estimate is smaller although $\partial N_2O/\partial O_3$ is larger in the model because the N_2O fields produced by the trajectory calculations are more similar to the model fields at 450K than at 500K. This analysis method does not indicate a systematic error at 400K.

The error estimates using GEOS DAS meteorological fields are combined with model ozone, and time series for (model + error - observation) are given for DIAL, POAM and MLS observations at each potential temperature surface in Plate 5. The model fields are from the Case II initialization as in Figure 3. Comparison with Plate 3 shows the net impact of the errors in model vertical advection due to the misrepresentation of the model profile shape and due to the systematic overestimate of the vertical velocity. At 400K, there is no significant change in the agreement between

model and observation, as the vertical transport is minimal. At 450K, agreement between model and observations is improved markedly. For POAM data, the mean of the square of the difference between the model and the observations is reduced from more 0.65 ppmv (Case I) to less than 0.4 ppmv (Case II no error estimate) to less than 0.15 ppmv (Case II with error estimate). At 500K the growing bias (evident in Plate 3, reduced but evident in Figure 3) is near zero until January 15. Because the model vertical gradient at 500K on December 9 is significantly larger than indicated in the DIAL data, the discrepancy at the end of January may due to an overestimate of the downward transport that is not accounted for in this analysis.

6. Summary and Conclusions

Analysis of the CTM results for high latitude northern hemisphere ozone evolution reveals significant uncertainties in the model ozone transport within the polar vortex. Comparison of the model ozone profile with profiles observed by DIAL showed a systematic tendency to overestimate the downward transport due to an overestimate of the model ozone vertical gradient. This was quantified by repeating the CTM calculation for an initial ozone field constrained to match the shape of December DIAL observations.

The CTM retains information about the initial profile throughout the integration, which suggests that there is not much exchange of air between the model vortex and midlatitudes or vertical mixing during December 1995 and January 1996, in agreement with most dynamical studies [*Schoeberl et al.*, 1992]. From the sense of these results, we

infer that the model profile must match observations during the formation period for the polar vortex for comparisons with observations, whether the model is utilized for a long (multi-year) integration or short seasonal calculations as presented here. The difference between the vertical gradient of DIAL profiles and the POAM profiles indicates the need for high vertical resolution observations to minimize uncertainty in the analysis. In the absence of such observations to verify the ozone vertical profile, the sensitivity of the ozone tendency to the profile shape must be accounted for when evaluating the completeness of the model chemistry.

The model vertical motion represents a second source of transport uncertainty. Diabatic trajectory calculations were used to determine the consistency of the model vertical transport with the heating rates. These calculations show that the vortex average decrease in N_2O from the CTM is generally larger than the decrease that would be consistent with heating rate calculations during December and January. This difference contributes to a systematic overestimate of the vertical transport of model ozone, and leads to an increase in model ozone relative to observations. The estimated transport errors exhibit the same temporal character as the bias between model and observation, and are of comparable magnitude. This is in contrast to the temporal character of the model sensitivity to total Cl_Y, which depends on insolation. The estimated errors using GEOS DAS input are larger than those using UKMO input, which also suggests a level of uncertainty in quantification of the transport contribution to the ozone tendency. When these systematic errors are accounted for, time series of the difference between the model and observations for the period December 1, 1995 -

January 31, 1996 exhibit little or no temporal dependence at 400K, 450K, and 500K.

This study reveals the importance of including a quantitative estimate of the transport uncertainty when attempting to make quantitative estimate of photochemical loss from observations through comparisons with a CTM simulation. These results do not support the need to include an additional midwinter ozone loss process in the CTM.

References

Albritton, D. L., and R. T. Watson, Co-Chairs, Scientific Assessment of Ozone Depletion: 1991, *World Meteorological Organization Global Ozone Research and Monitoring Project - Report No. 25*, 1992.

Albritton, D. L., R. T. Watson, and P. J. Aucamp, Co-Chairs, Scientific Assessment of Ozone Depletion: 1994, *World Meteorological Organization Global Ozone Research and Monitoring Project - Report No. 37*, 1995.

Anderson, D. E., Jr., and S. A. Lloyd, Polar twilight UV-visible radiation field: perturbations due to multiple scattering, ozone depletion, stratospheric clouds, and surface albedo, *J. Geophys. Res., 95*, 7429-7434, 1990.

Anderson, J. G., D. W. Toohey, and W. H. Brune, Free radicals within the Antarctic vortex: the role of CFCs in the Antarctic ozone loss, *Science, 251*, 39-46, 1991.

Andrews, D. G., and M. E. McIntyre, Planetary waves in horizontal and vertical shear: The generalized Eliassen-Palm relation and the mean zonal acceleration, *J. Atmos. Sci., 33*, 2031-2048, 1976.

Barath, F., et al., The upper atmosphere research satellite microwave limb sounder instrument, *J. Geophys. Res., 98*, 10751-10762, 1993.

Becker, G., R. Müller, D. McKenna, M. Rex, and K. S. Carslaw, Ozone loss rates in the Arctic stratosphere in the winter 1991-1992: Model calculations compared with Match results, *Geophys. Res. Lett., 25*, 4325-4328, 1998.

Browell, E. V., S. Ismail, and W. B. Grant, Differential absorption lidar (DIAL) measurements from air and space, *APpl. Phys. B67*, 299-410, 1998.

Brune, W. H., D. W. Toohey, J. G. Anderson, and K. R. Chan, In situ observations of ClO in the Arctic stratosphere: ER-2 aircraft results from 59°N to 80°N latitude, *Geophys. Res. Lett., 17*, 505-508, 1990.

Chipperfield, M. P., Multiannual simulations with a three-dimensional chemical transport model, *J. Geophys. Res., 104*, 1781-1805, 1999.

Coy, L., E. R. Nash, and P. A. Newman, Meteorology of the polar vortex: Spring 1997, *Geophys. Res. Lett., 24*, 2693-2696, 1997.

Data Assimilation Office, Algorithm theoretical basis document version 1.01, Data Assimilation Office, NASA Goddard Space Flight Center, Greenbelt, MD., 1997.

DeMore, W. B., et al., Chemical kinetics and photochemical data for use in stratospheric modeling, Evaluation number 11, *JPL Publ. 94-20*, 1994.

DeMore, W. B., et al., Chemical kinetics and photochemical data for use in stratospheric modeling, Evaluation number 12, *JPL Publ. 97-4*, 1997.

Deniel, C., R. M. Bevilacqua, J. P. Pommereau, and F. Lefevre, Arctic chemical ozone depletion during the 1994-95 winter deduced from POAM II satellite observations and the REPROBUS three-dimensional model, *J. Geophys. Res., 103*, 19,231-19,244, 1998.

Douglass, A. R., C. J. Weaver, R. B. Rood and L. Coy, A three-dimensional simulation

of the ozone annual cycle using winds from a data assimilation system, *J. Geophys. Res., 101*, 1463-1474, 1996.

Douglass, A. R., R. B. Rood, S. R. Kawa, and D. J. Allen, A three dimensional simulation of the middle latitude winter ozone in the middle stratosphere, *J. Geophys. Res., 102*, 19,217-19,232, 1997.

Douglass, A. R., and S. R. Kawa, Contrast between 1992 and 1997 high-latitude spring Halogen Occultation Experiment observations of lower stratospheric HCl, *J. Geophys. Res., 104*, 18,739-18,754, 1999.

Dunkerton, T., On the mean meridional mass motions of the stratosphere and mesosphere, *J. Atmos. Sci., 35*, 2325-2333, 1978.

Farman, J. C., B. G. Gardiner, and J. D. Shanklin, Large losses of total ozone in Antarctica reveal seasonal ClO_x/NO_X interaction, *Nature, 315*, 207-210, 1985.

Froidevaux, L., et al., Validation of UARS Microwaves Limb Sounder ozone measurements, *J. Geophys. Res., 101*, 10,017-10,060, 1996.

Glaccum, W., et al., The Polar Ozone and Aerosol Measurement (POAM II) instrument, *J. Geophys. Res., 101*, 14,479-14,487, 1996.

Goutail, F., et al., Depletion of column ozone in the Arctic during the winters of 1993-94 and 1994-95, *J. Atmos. Chem., 32*, 1-34, 1999.

Grant, W. B., M. A. Fenn, E. V. Browell, T. J. McGee, U. N. Singh, M. R. Gross, I. S. McDermid, L. Froidevaux and P.-H. Wang, Correlative stratospheric

ozone measurements with the airborne UV DIAL system during TOTE/VOTE, *Geophys. Res. Lett., 25*, 623-626, 1998.

Jackman, C. H., E. L. Fleming, S. Chandra, D. B. Considine, and J. E. Rosenfield, Past, present, and future modeled ozone trends with comparisons to observed trends, *J. Geophys. Res., 101*, 28,753-28,767, 1996.

Kawa, S. R., J. B. Kumer, A. R. Douglass, A. E. Roche, S. E. Smith, F. W. Taylor, and D. J. Allen, Missing chemistry of reactive nitrogen in the upper stratospheric polar winter, *Geophys. Res. Lett., 22*, 2629-2632, 1995.

Kawa, S. R., et al., Activation of chlorine in sulfate aerosol as inferred from aircraft observations, *J. Geophys. Res., 102*, 3921-3933, 1997.

Lefevre, F., F. Figarol, K. S. Carslaw, T. Peter, The 1997 Arctic ozone depletion quantified from three-dimensional model simulations, *Geophys. Res. Lett., 25*, 2425-2428, 1998.

Lin, S. J., and R. B. Rood, Multidimensional flux form semi-Lagrangian transport schemes, *Mon. Wea. Rev., 124*, 2046-2070, 1996.

Lumpe, J. D., R. M. Bevilacqua, K. W. Hoppel, S. S. Krigman, C. Brogniez, E. P. Shettle and D. Kriebel, POAM II retrieval algorithm and error analysis, *J. Geophys. Res., 102*, 23,593-23,614, 1997.

Manney, G. L., L. Froidevaux, J. W. Waters, R. W. Zurek, W. G. Read, L. S. Elson, J. B. Kumer, J. L. Mergenthaler, A. E. Roche, A. O'Neill, R. S. Harwood, I.

MacKenzie, and R. Swinbank, Chemical depletion of ozone in the Arctic lower stratosphere during winter 1992-93, *Nature, 370,* 429-434, 1994.

Manney, G. L., L. Froidevaux, J. W. Waters, M. L. Santee, W. G. Read, D. A. Flower, R. F. Jarnot, and R. W. Zurek, Arctic ozone depletion observed by UARS MLS during the 1994-1995 winter, *Geophys. Res. Lett., 23,* 85-88, 1996.

Müller, R., J.-U. Grooss, D. S. McKenna, P. J. Crutzen, C. Brühl, J. M. Russell III, and A. F. Tuck, HALOE observations of the vertical structure of chemical ozone depletion in the Arctic vortex during winter and early spring 1996-1997, *Geophys. Res. Lett., 24,* 2717-2720, 1997.

Nash, E. R., P. A. Newman, J. E. Rosenfield and M. R. Schoeberl, An objective determination of the polar vortex using Ertel's potential vorticity, *J. Geophys. Res., 101,* 9471-9478, 1996.

Newman, P. A., J. F. Gleason, R. D. McPeters, and R. S. Stolarski, Anomalously low ozone over the Arctic, *Geophys. Res. Lett., 24,* 2689-2692, 1997.

Rex., M. et al., In situ measurements of stratospheric ozone depletion rates in the Arctic winter 1991/92; a Lagrangian approach, *J. Geophys. Res.,* in press 1998.

Rex., M. et al., Chemical ozone loss in the Arctic winer 1994/95 as determined by the MATCH technique, *J. Atmos. Chem., 32,* 35-59, 1999.

Reber, C. A., C. E. Trevathan, R. J. McNeal, and M. R. Luther, The Upper Atmosphere Research Satellite (UARS) mission,*J. Geophys. Res., 98,*10,643-10,647, 1993.

Rosenfield, J. E., P. A. Newman and M. R. Schoeberl, Computations of diabatic descent in the stratospheric polar vortex, *J. Geophys. Res., 99*, 16,677-16,689, 1994.

Santee, M. L., G. L. Manney, W. G. Read, L. Froidevaux, and J. W. Waters, Polar vortex conditions during the 1995-96 Arctic winter: MLS ClO and HNO_3, *Geophys. Res. Lett., 23*, 3207-3210, 1996.

Schoeberl, M. R., M. H. Proffitt, K. K. Kelly, L. R. Lait, P. A. Newman, J. E. Rosenfield, M. Loewenstein, J. R. Podolske, S. E. Strahan, and K. R. Chan, Stratospheric constituent trends from ER-2 profile data, *J. Geophys. Res., 17*, 469-472, 1990.

Schoeberl, M. R., and L. R. Lait, Conservative coordinate transformations using atmospheric measurements, in *The Use of EOS for Studies of Atmospheric Physics*, edited by G. Visconti and J. Gille, pp. 419-430, North-Holland, New York, 1992.

Schoeberl, M. R., L. R. Lait, P. A. Newman and J. E. Rosenfield, The structure of the polar vortex, *J. Geophys. Res.,97*, 7859-7882, 1992.

Solomon, S., Progress towards a quantitative understanding of Antarctic ozone depletion, *Nature, 347*, 347-354, 1990.

Stolarski, R. S. et al. 1995 scientific assessment of the atmospheric effects of stratospheric aircraft, *NASA Ref. Publ. 1381*, 1995.

Waters, J. W., G. L. Manney, W. G. Read, L. Froidevaux, D. A. Flower, and R. F. Jarnot, UARS MLS observations of lower stratospheric ClO in the 1992-93 and 1993-94 Arctic winter vortices, *Geophys. Res. Lett., 22*, 823-826, 1995.

Waters, J. W., et al., Validation of UARS MLS ClO measurements, *J. Geophys. Res., 101*, 10091-10127, 1996.

Weaver, C. J., A. R. Douglass and R. B. Rood, Thermodynamic balance of three-dimensional stratospheric winds derived from a data assimilation procedure, *J. Atmos. Sci., 50*, 2977-2993, 1993.

Wu, J. and A. Dessler, submitted to *J. Geophys. Res.,*, 2000.

Received _____

Figure 1. Sunlit MLS ClO (+) is compared with an estimate of model ClO. Averages are calculated for all MLS points with potential vorticity greater than that at 70°N equivalent latitude. The vertical bars are the standard deviation of MLS observations. The temporal dependence of model ClO matches that of MLS ClO. The lines represent the model ClO_x binned and averaged using equivalent latitude, and show that in the model ClO_x is nearly uniform across the vortex.

Figure 2. (a) The average of December observations from DIAL, MLS and POAM at 500 K is 0.3-0.5 ppmv lower than the average of model values at the time and location of the observations. (b) Same as (a) but for January 24 - February 19. There is a significant bias for equivalent latitudes greater than 66°N that is not apparent in the December comparison.

Figure 3. (a) The differences at 500K between the model and MLS are consistent with the differences between the model and POAM, and are smaller for Case II initialization than shown in Plate 3. (b) The difference between the model for Case I and Case II (crosses) and Case II and Case III (diamonds) show that during this time period the model is much more sensitive to the vertical advection than to the model photochemistry.

Figure 4. (a) For 500K, the estimated errors in the ozone simulation due to differences in the model vertical transport diagnosed using diabatic trajectories using GEOS DAS data for seven 15 day periods; (b) Same as (a) using UKMO data; (c) The accumulated error in O_3 which should be taken into account in comparing simulated O_3 with observations calculated from GEOS DAS data (d) Same as (c) using UKMO data

Plate 1. (a) The DC-8 flight track (solid black line between 200 and 280 longitude near 67°N), POAM (white filled circles) and MLS (small purple stars), all on January 30, 1996, are superposed on the model N_2O at 500K to show that each platform makes measurements within vortex and middle latitude air. (b) The model N_2O exhibits a strong correlation with the potential vorticity at 500K.

Plate 2. (a) Average model profile for Case I initialization sampled at the time and location of observations compared with profiles from DIAL, MLS, and POAM for December 1995; (b) Same as (a) but for Case II initialization (c) Vertical derivative of the profiles in (a); (d) Vertical derivative of the profiles in (b)

Plate 3. (a) Time series at 400K for model - DIAL, averaged by equivalent latitude for Case I initialization; (b) Same as (a) but for 450K; (c) same as (a) but for 500K; (d) same as (a) but for model - POAM; (e) same as (d) but for 450K; (f) same as (d) but for 500K; (g) Same as (f) but for MLS.

Plate 4. (a) CTM N_2O at 500K for December 31, 1995; (b) N_2O at 500K by mapping CTM N_2O from December 16, 1995 to the December 31, 1995 initial grid for back trajectories using GEOS DAS fields; (c) same as (b) using UKMO fields (d) same as (a) January 31, 1996; (e) same as (b) but mapping January 16, 1996 to January 31, 1996; (f) same as (e) but for UKMO fields

Plate 5. (a) Time Series for the difference model - DIAL at 400K for Case II initialization (black) accounting for error estimate from GEOS DAS (green); (b) same as (a) at 450K; (c) same as (a) at 500K; (d) same as (a) but for POAM; (e) same as (b) but for POAM; (f) same as (c) but for POAM; (g) same as (f) but for MLS

Table 1. DC-8 Flight Information

Date	Latitudes	Longitudes	Duration
December 8 1995	41°N-66°N	216°E-244°E	5 hr
December 9, 1995	67°N-83dgN	190°E-321°E	9 hr
December 11, 1995	60°N-20°N	202°E-209°E	6 hr
January 24, 1996	43°N-65°N	221°E-265°E	6 hr
January 28, 1996	68°N-90°N	211°E-303°E	6 hr
January 30, 1996	65°N-68°N	220°E-278°E	6 hr
February 1, 1996	66°N-80°N	219°E-334°E	5 hr
February 4, 1996	67°N-77°N	218°E-244°E	2 hr
February 8, 1996	59°N-23°N	200°E-208°E	6 hr

500K Jan. 30 1996

(a) Model N2O

(b) GEOS DAS EPV

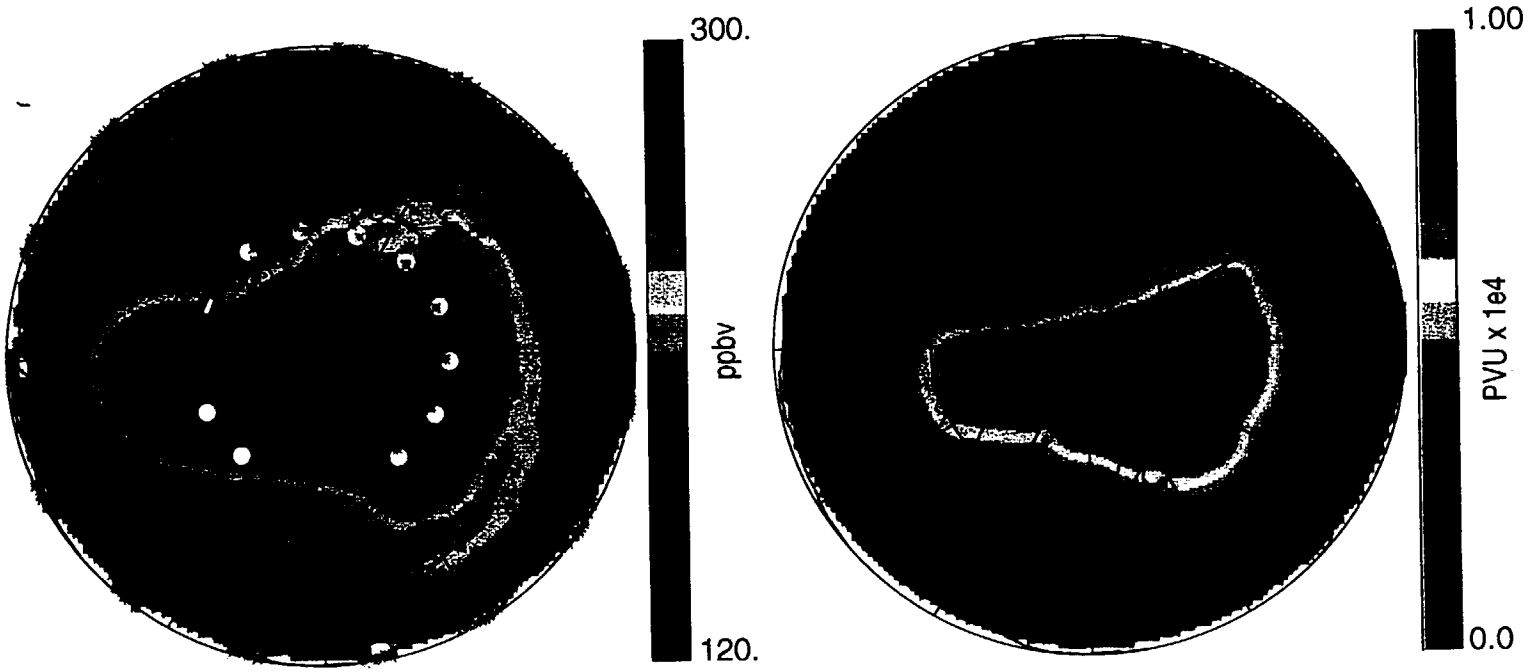

Plate 1

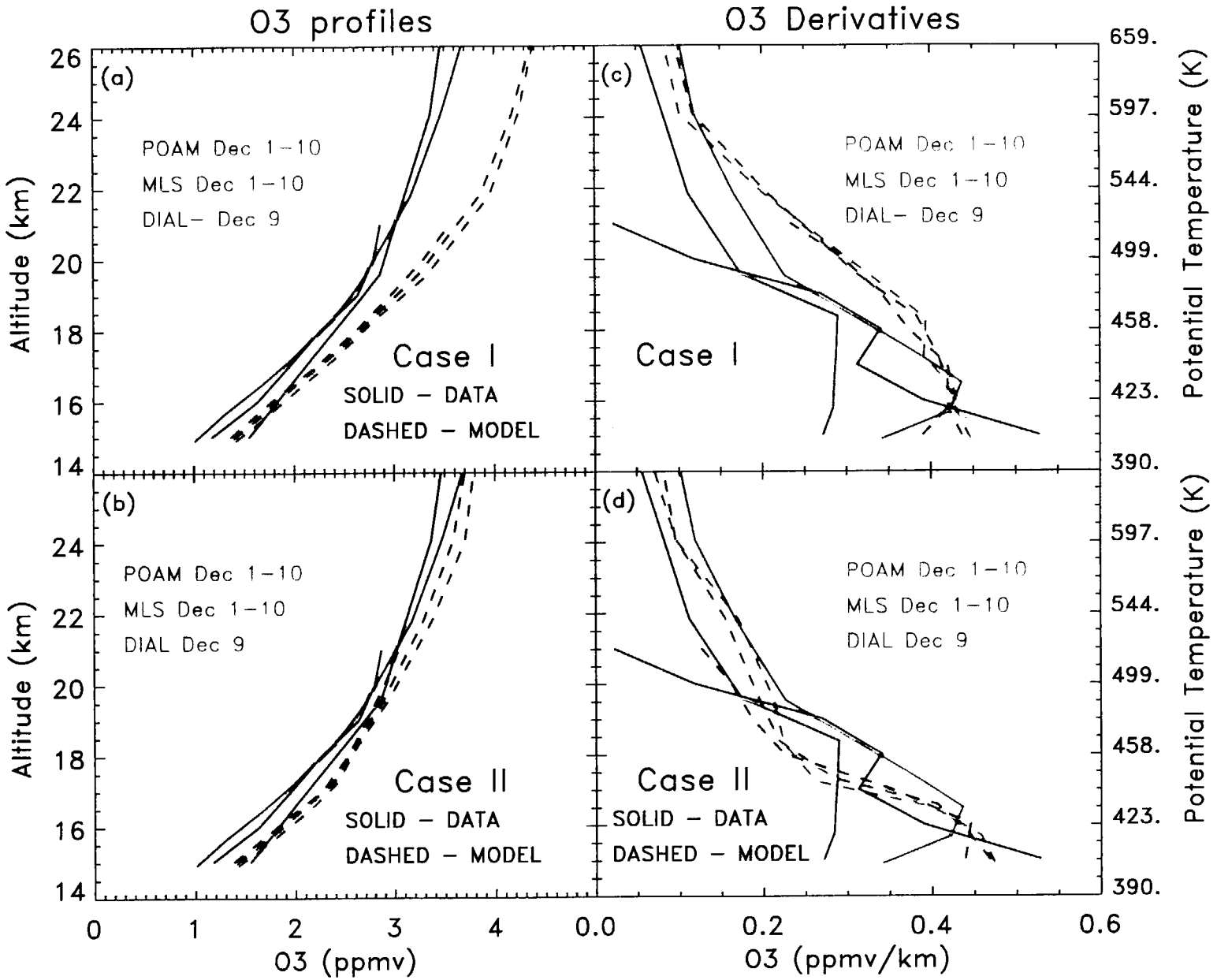
O3 profiles
O3 Derivatives
(a)
(b)
(c)
(d)
POAM Dec 1–10
MLS Dec 1–10
DIAL– Dec 9
DIAL Dec 9
Case I
Case II
SOLID – DATA
DASHED – MODEL
Altitude (km)
Potential Temperature (K)
O3 (ppmv)
O3 (ppmv/km)
26
24
22
20
18
16
14
659.
597.
544.
499.
458.
423.
390.
0
1
2
3
4
0.0
0.2
0.4
0.6

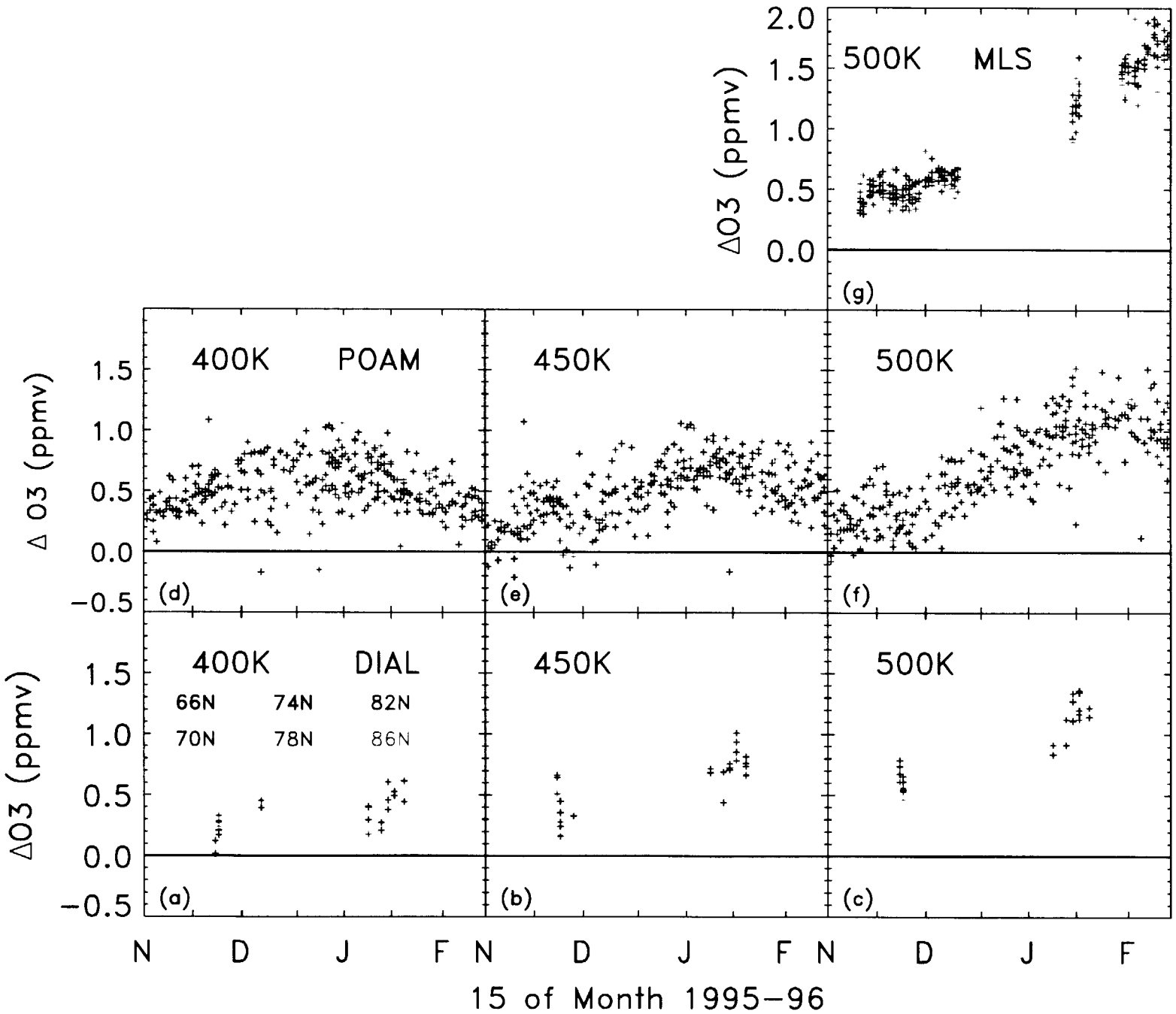
500K MLS
(g)
400K POAM
450K
500K
(d)
(e)
(f)
400K DIAL
66N 74N 82N
70N 78N 86N
450K
500K
(a)
(b)
(c)
Δ 03 (ppmv)
Δ03 (ppmv)
2.0
1.5
1.0
0.5
0.0
−0.5
N D J F N D J F N D J F
15 of Month 1995−96

Plate 3

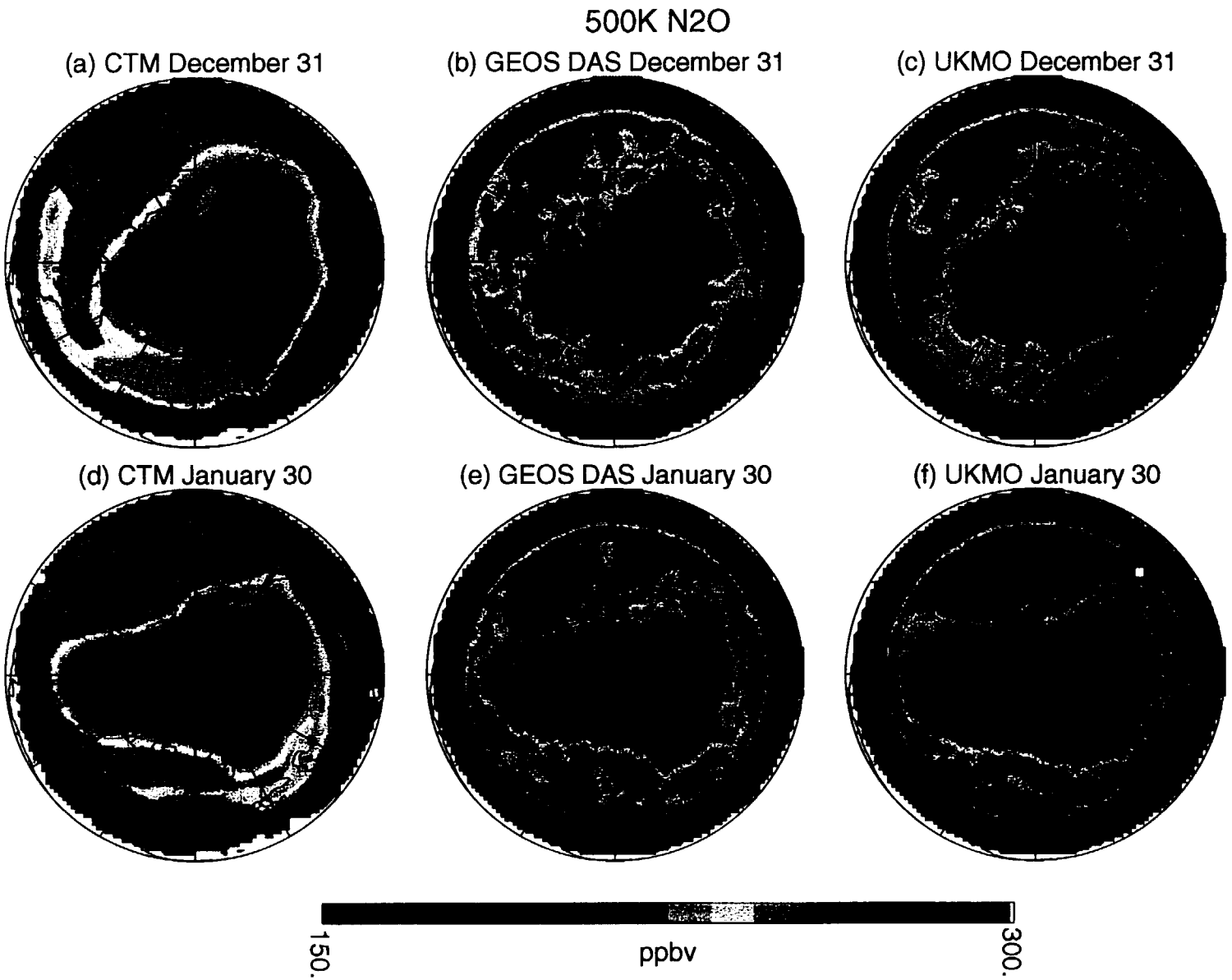
500K N2O
(a) CTM December 31
(b) GEOS DAS December 31
(c) UKMO December 31
(d) CTM January 30
(e) GEOS DAS January 30
(f) UKMO January 30
150.
ppbv
300.

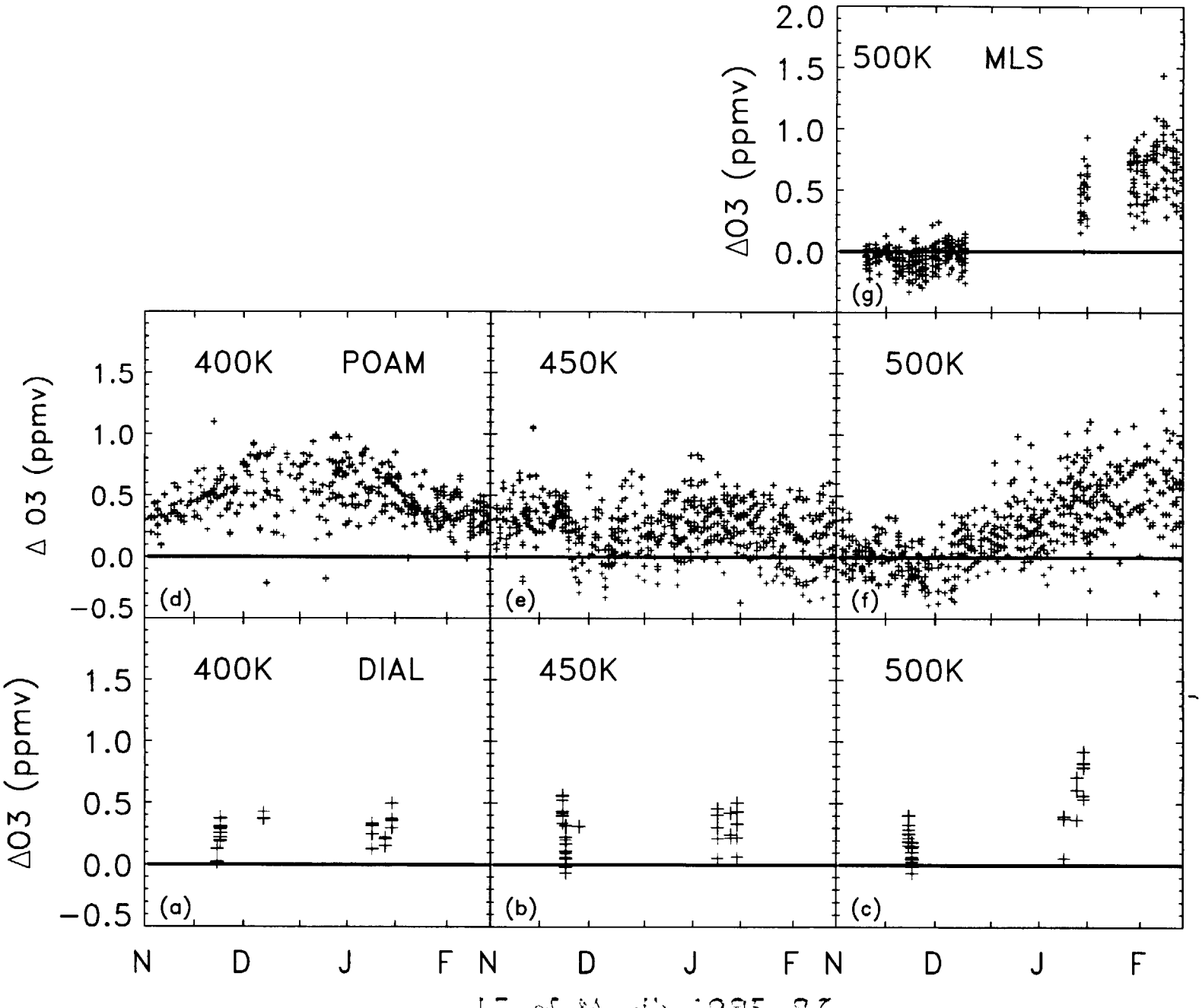
500K MLS
(g)
400K POAM
(d)
450K
(e)
500K
(f)
400K DIAL
(a)
450K
(b)
500K
(c)
Δ 03 (ppmv)
Δ03 (ppmv)
2.0
1.5
1.0
0.5
0.0
−0.5
N D J F N D J F N D J F
15 of Month 1995-96

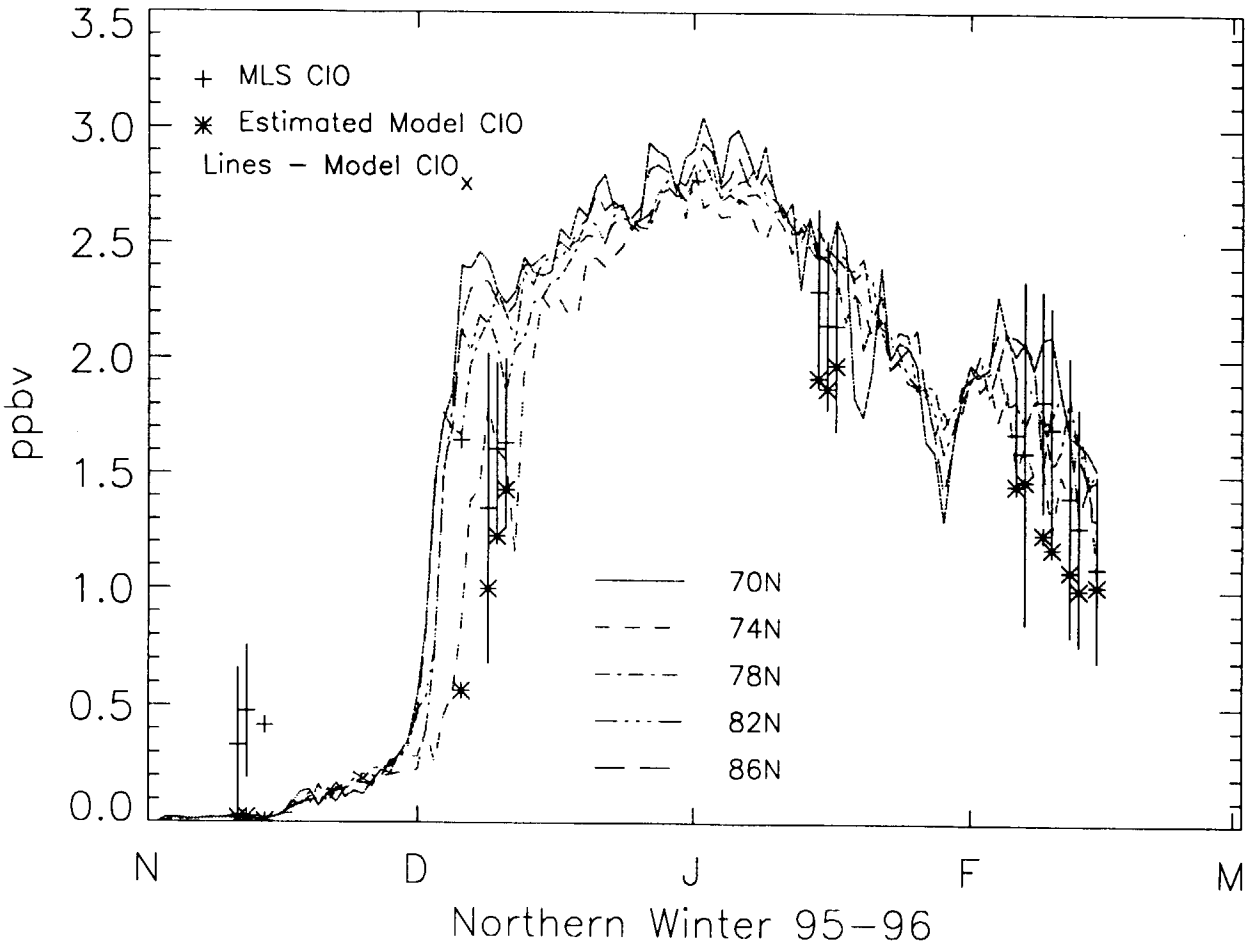
+ MLS ClO
* Estimated Model ClO
Lines – Model ClO$_x$
70N
74N
78N
82N
86N
ppbv
3.5
3.0
2.5
2.0
1.5
1.0
0.5
0.0
N
D
J
F
M
Northern Winter 95–96

Figure 1

Case I Initialization

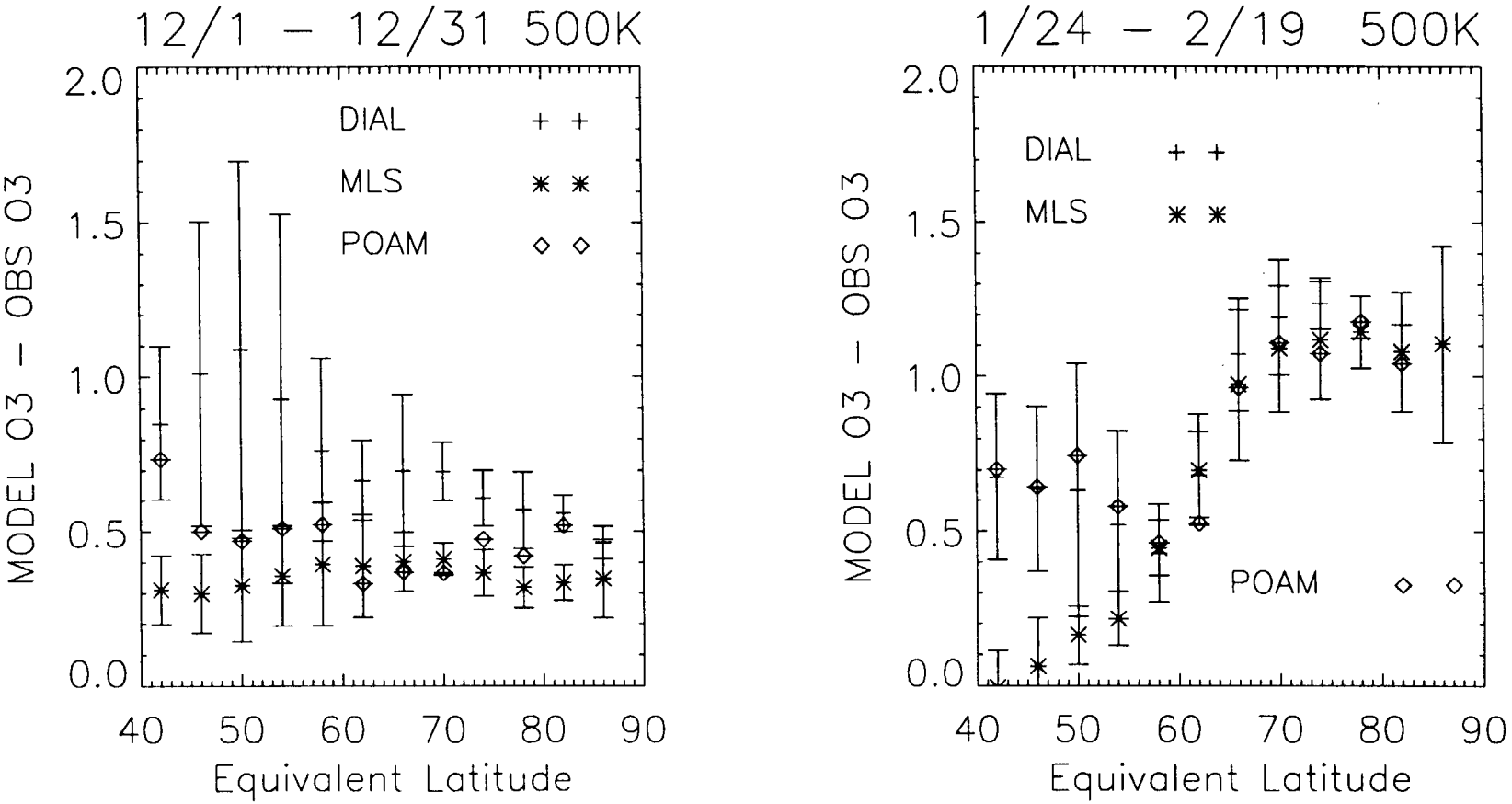

Figure 2

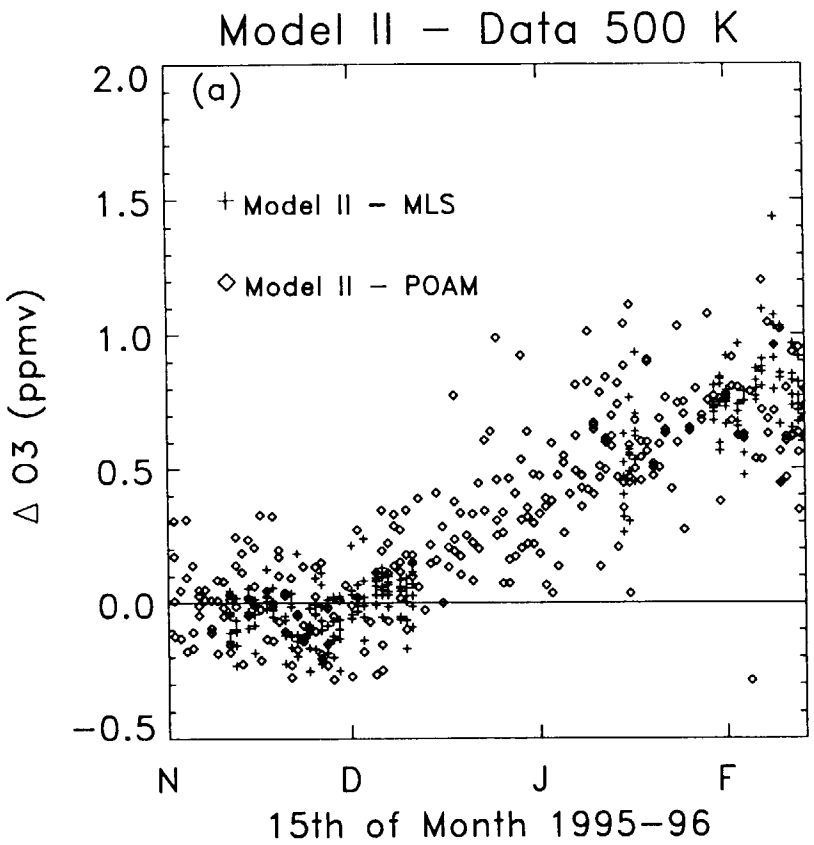
Model II − Data 500 K
(a)
+ Model II − MLS
◇ Model II − POAM
Δ O3 (ppmv)
2.0
1.5
1.0
0.5
0.0
−0.5
N
D
J
F
15th of Month 1995−96

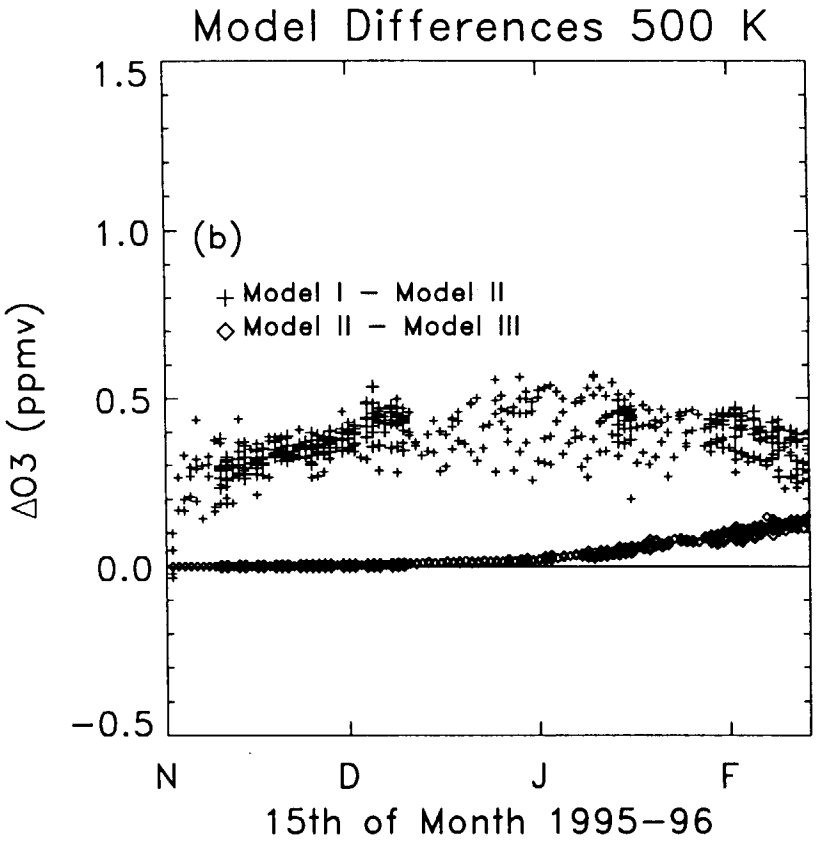
Model Differences 500 K
(b)
+ Model I − Model II
◇ Model II − Model III
ΔO3 (ppmv)
1.5
1.0
0.5
0.0
−0.5
N
D
J
F
15th of Month 1995−96

Figure 3

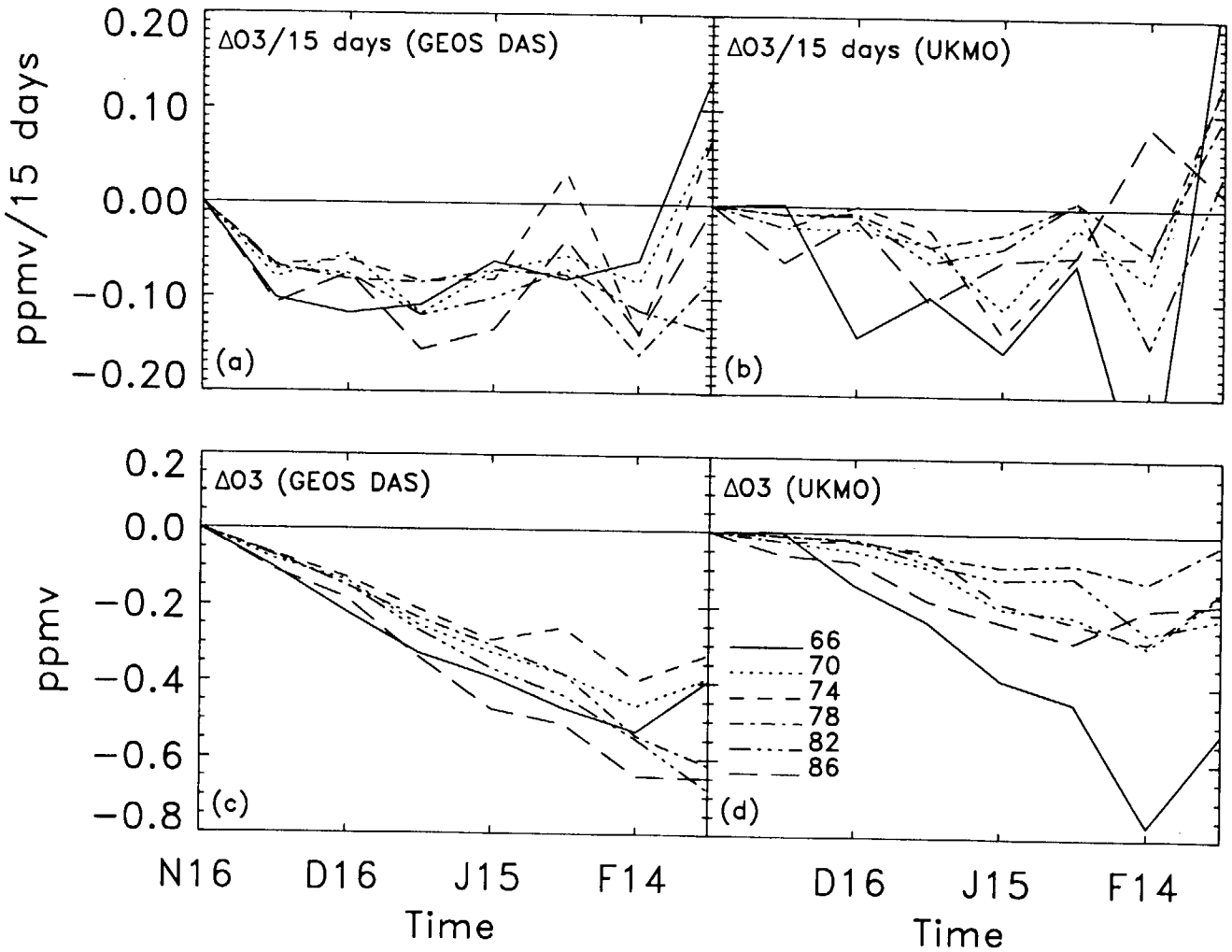
0.20
0.10
0.00
−0.10
−0.20
ppmv/15 days
ΔO3/15 days (GEOS DAS)
ΔO3/15 days (UKMO)
(a)
(b)
0.2
0.0
−0.2
−0.4
−0.6
−0.8
ppmv
ΔO3 (GEOS DAS)
ΔO3 (UKMO)
66
70
74
78
82
86
(c)
(d)
N16
D16
J15
F14
D16
J15
F14
Time
Time